2022

Gene Electrotransfer of FGF2 Enhances Collagen Scaffold Biocompatibility

Carly Boye

Kyle Cristensen

Kamal Asadipour
Old Dominion University, kasadipo@odu.edu

Scott DeClemente
Old Dominion University

Michael Francis

See next page for additional authors

Original Publication Citation

Boye, C., Christensen, K., Asadipour, K., DeClemente, S., Francis, M., & Bulysheva, A. (2022). Gene electrotransfer of FGF2 enhances collagen scaffold biocompatibility. *Bioelectrochemistry*, 144, 1-11, Article 107980. https://doi.org/10.1016/j.bioelechem.2021.107980

Bioelectrochemistry 144 (2022) 107980

Contents lists available at ScienceDirect

Bioelectrochemistry

journal homepage: www.elsevier.com/locate/bioelechem

Gene electrotransfer of FGF2 enhances collagen scaffold biocompatibility

Carly Boye [a], Kyle Christensen [b], Kamal Asadipour [c], Scott DeClemente [c], Michael Francis [d], Anna Bulysheva [c,*]

[a] Center for Molecular Medicine and Genetics, Wayne State University, Detroit, MI, United States
[b] Embody Inc., Norfolk, VA, United States
[c] Department of Electrical and Computer Engineering, Old Dominion University, Norfolk, VA, United States
[d] Asante Bio, Norfolk, VA, United States

ARTICLE INFO

Article history:
Received 31 January 2021
Received in revised form 19 September 2021
Accepted 7 October 2021
Available online 29 October 2021

Keywords:
Gene therapy
Gene electrotransfer
Collagen bioprinting
Tendon regeneration
Angiogenesis
Biocompatibility

ABSTRACT

Tendon injuries are a common athletic injury that have been increasing in prevalence. While there are current clinical treatments for tendon injuries, they have relatively long recovery times and often do not restore native function of the tendon. In the current study, gene electrotransfer (GET) parameters for delivery to the skin were optimized with monophasic and biphasic pulses with reporter and effector genes towards optimizing underlying tendon healing. Tissue twitching and damage, as well as gene expression and distribution were evaluated. Bioprinted collagen scaffolds, mimicking healthy tendon structure were then implanted subcutaneously for biocompatibility and angiogenesis analyses when combined with GET to accelerate healing. GET of human fibroblast FGF2 significantly increased angiogenesis and biocompatibility of the bioprinted implants when compared to implant only sites. The combination of bioprinted collagen fibers and angiogenic GET therapy may lead to better graft biocompatibility in tendon repair.

1. Introduction

Internationally, the incidence of Achilles tendon ruptures has been increasing over time as shown by several studies published between 1996 and 2016 [1–5]. In the U.S., between 2007 and 2011 approximately 106 out of 100,000 people experienced an incidence of Achilles tendinopathy [6]. Achilles tendinopathy affects many facets of the population. Acute Achilles tendon ruptures often occurs during athletic activity; however, chronic Achilles tendinopathy can occur in non-athletes and is often related to overuse or other medical conditions [7]. Two main forms of chronic Achilles tendinopathy exist: non-insertional and insertional. Non-insertional Achilles tendinopathy is caused by impairment to circulation and edema [7]. Insertional Achilles tendinopathy is often seen in older patients or those with underlying conditions such as obesity or diabetes [7].

Current clinical treatments for Achilles tendon injury include non-surgical and surgical methods [8]. Non-surgical treatment protocols may vary between mobilization and immobilization, as well as weight-bearing and non-weight-bearing rehabilitation therapies [8]. Surgery has been the preferred treatment due to high re-rupture rates in non-surgical treatments [7,8]. Surgical treatments can include a FiberWire® method [9] or a graft method [10]. The FiberWire® method is subject to issues with the knots unravelling [9], while the graft method is more subject to issues regarding strength of the tendon after treatment [10]. Surgery also carries many undesirable risks such as infection, complications such as deep vein thrombosis, and nerve injury [8]. Additionally, recovery times for surgery are typically at least 1 month, in which the patient cannot move or bear weight on the injured tendon [8]. The time of recovery is particularly important in Achilles tendinopathy as the condition obstructs basic movements such as walking and jumping [8]. Neither of these methods restore mechanical strength or structure that the tendon had prior to injury [11]. Additionally, surgical and non-surgical outcomes vary in terms of risk of re-rupture and other complications [7,8].

There are several alternative tendinopathy treatment methods currently being researched, including laser therapies, steroid therapies, various types of gene and growth factor therapies [11], and bioengineered scaffolds [12,13]. Gene and growth factor therapies largely focus on aiding at least one of the three steps of the tendon-healing process: inflammation, proliferation, and remodeling [11]. Bioengineered scaffold treatments often address the issue of maintaining a similar structure and strength to native tendons [12]. This

* Corresponding author.
E-mail address: abulyshe@odu.edu (A. Bulysheva).

https://doi.org/10.1016/j.bioelechem.2021.107980
1567-5394/

study focuses on integrating a bioengineered scaffold in conjunction with gene therapy facilitating early angiogenesis and improved healing.

3D bioprinted collagen scaffolds are currently of large interest in tissue engineering research [13]. Collagen type I can be produced on a large scale and is generally biocompatible and biodegradable [13]. These scaffolds have been shown to support cell attachment and proliferation [13]. Some designs also provide similar mechanical strength to native tendons [12]. Additionally, tendons are primarily composed of highly aligned collagen type I bundles, therefore, our biomimetic tendon graft was specifically designed to also be composed of highly aligned collagen type I wet-extruded microfibers.

Many gene delivery methods are available but can be divided into two major categories: viral and non-viral [14]. Viral gene delivery offers high transfection efficiency and improved gene expression levels, however there are also safety concerns with using viral vectors, such as immunogenicity and insertional mutagenesis [14].

Gene electrotransfer (GET) is an established non-viral, physical method of gene delivery. Electric pulses are applied to the tissue of interest and the cells are temporarily permeabilized, allowing larger molecules such as plasmid DNA to enter the cells. Previous work has shown that GET is an effective method for gene delivery to the skin, resulting in significantly increased gene expression when compared to naked plasmid DNA injection only (IO) [15–17]. However, there are several drawbacks to existing methods. Often high voltage and long (millisecond-scale) pulses are required for efficient delivery, however, typically if voltage is reduced to minimize tissue damage, transfection efficiency is also reduced. Combination of low voltage and applied heating have been reported, however the technology requires more specialized equipment (i.e. IR laser heating) [15,17]. Therefore, the current study focused on achieving higher levels of expression without the use of additional aids such as heat or plasma, to increase gene expression levels [15,17]. Additionally, a parallel plate electrode configuration was used to create a uniform electric field at the site of gene delivery. For GET, we adapted biphasic pulsing parameters, which have been previously reported to reduce skeletal muscle twitching during irreversible electroporation [18,19].

GET has previously been used in conjunction with 3D cell culture models for multiple applications, studying biologic mechanisms and processes *in vitro* models more closely representing *in vivo* conditions [20–23]. Spheroid culture is a well-established 3D cell culture method in conjunction with electroporation. More recently, various scaffolds have been used in conjunction with electroporation [22,23], as spheroids are heterogenous in size [24] which affects their electrical properties [25]. A recent study specifically investigated the use of GET with a collagen scaffold *in vitro* [22]. This study showed the collagen scaffold had increase transfection efficiency compared to 2D culture, and the authors suggest that this method could be used to optimize *in vivo* GET protocols [22]. Additionally, GET has been suggested for promotion of blood vessel development with tissue engineering applications [26,27]. In the present work, we show that biocompatibility can be improved with angiogenic growth factor gene delivery enhanced by biphasic GET.

Fibroblast growth factors are a group of growth factors that regulate many biological processes associated with tissue repair and regeneration [28]. Basic fibroblast growth factor (also fibroblast growth factor 2 or FGF2) is involved with several related functions, including cell proliferation, cell migration, cell differentiation, and angiogenesis [28]. Angiogenesis is critical for tissue remodeling and repair [11]. Because of this, many gene therapy approaches deliver a gene or genes that are associated with angiogenesis [11]. Previous studies in rat and rabbit models used GET to deliver FGF2 [29,30]. Both studies found that delivery of FGF2 induced angiogenesis [29,30]. FGF2 is also involved in the proliferation and remodeling portions of the tendon-healing process [11]. It is well known that hypovascular tissues heal poorly, therefore we hypothesize that induction of early angiogenesis, by expression of a potent angiogenic growth factor (FGF2) would enhance healing and graft integration. By using a collagen scaffold in conjunction with angiogenic gene therapy, our aim is to enhance oxygenation and biocompatibility of the collagen graft to improve tendon repair and healing after injury.

2. Materials and methods

2.1. Collagen I scaffold biofabrication

Collagen microfiber grafts were provided by Embody Inc (Norfolk, VA). Briefly, clinical-grade type I collagen microfiber (~150 μm diameter) was produced using a microfluidic wetspinning process as previously reported [36] and sterilized by electron beam sterilization prior to bioprinting. The fiber was controllably wrapped next to and on top of itself using a novel 3D bioprinting process that decorates the fibers with a cellular glue (hyaluronic acid, in these studies) to form a cohesive, multi-layer 3D constructs with designed geometries akin to native tendon tissue with aligned collagen fibers of high strength. These bioprinted constructs aim to mimic the biochemical, structural, and mechanical properties of musculoskeletal tissue for sports medicine indications.

The bioprinting process is capable of producing both acellular and cellularized grafts. For GET-focused studies herein, acellular ring-shaped grafts comprised of densely packed, highly parallel collagen microfiber were bioprinted and secured at each end with 6–0 Prolene ® suture (Fig. 1A). Sutured ends were not trimmed prior to implantation (as is shown in Fig. 1A) and instead left with needles attached in order to facilitate subcutaneous implantation, minimizing surgery time. When pulled taught by the sutured ends, grafts form a rectangular shape with approximately 9 mm length, 1.5 mm width, and 0.5 mm thickness. To facilitate graft formation, collagen fiber was coated with a 5 mg/mL hyaluronic acid (HA) solution prepared in DMEM supplemented with 2% ABAM (all sourced from Sigma-Aldrich, St. Louis, MO) during the bioprinting process.

Cellularized grafts were also produced to assess biocompatibility of the bioprinting process and the constituent collagen fiber *in vitro*. Briefly, human tenocytes (ZenBio, Durham, NC) were suspended at 4×10^6 cells/mL in the HA solution and deposited throughout grafts during the printing process. AlamarBlue ™ Assay (Thermo Fisher Scientific, Waltham, MA) for metabolic activity was conducted for grafts printed with human tenocytes after 1, 3, and 7 days in culture according to recommend manufacturer protocols (Fig. 1B). After 14 days in culture, grafts were stained with Invitrogen Molecular Probes VybrantTM DiD (Thermo Fisher Scientific, Waltham, MA) cytoplasmic labeling solution according to recommended manufacturer protocols. Epifluorescence imaging was performed using automated full focus and image haze reduction of the Keyence BZ-X800 microscope. DAPI and Cy5 channels were used to capture scaffold autofluorescence (Fig. 1C) and DiD-labeled tenocytes respectively (Fig. 1D). Imaging was performed at 20x magnification.

2.2. Animals

Male and female Sprague Dawley rats initially weighing 250–300 g purchased from Charles River Laboratories (Wilmington, MA) were used for this study. All animal studies followed an approved Old Dominion University Institutional Animal Care and

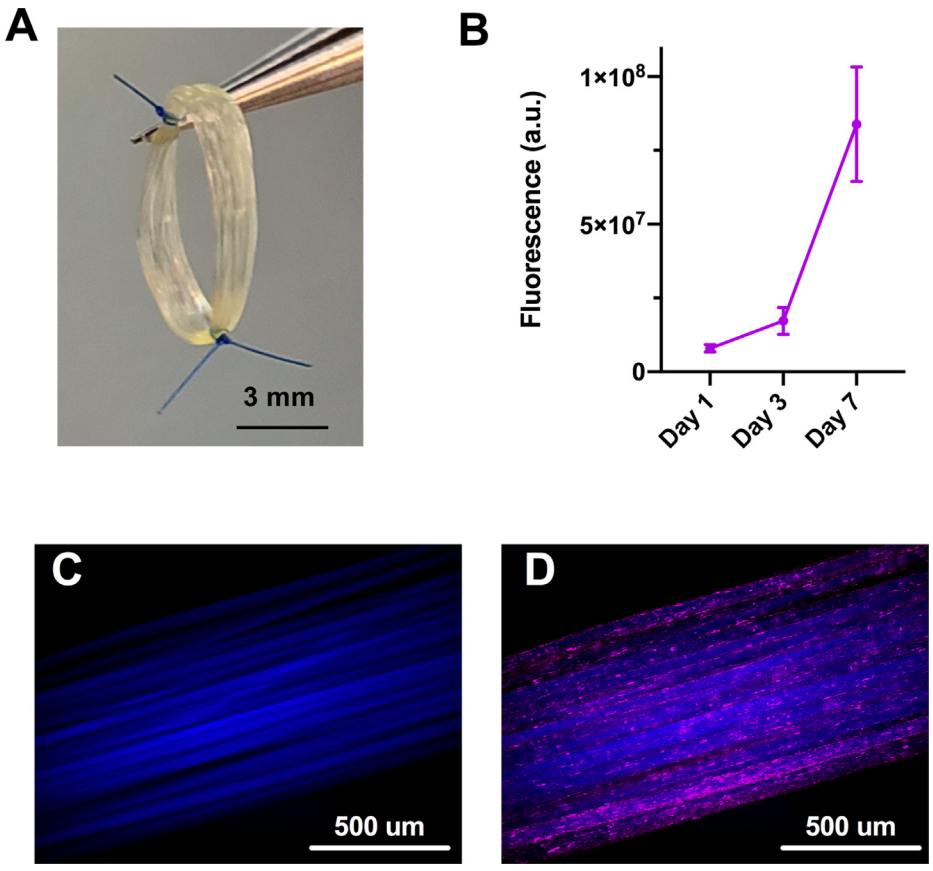

Fig. 1. Bioprinted grafts support cell viability during bioprinting and subsequent cell culture. An acellular bioprinted collagen microfiber graft secured at two ends with suture (A). Metabolic activity of grafts printed with human tenocytes exponentially increases 1, 3, and 7 days in culture (B). Error bars show standard deviation (n = 6). Fluorescence image of a cellularized bioprinted graft DAPI channel only (C) showing human tenocytes (magenta) with the cytoplasmic label DiD distributed throughout the aligned collagen fiber (blue) with bright autofluorescence at 405 nm (D). (For interpretation of the references to colour in this figure legend, the reader is referred to the web version of this article.)

Use Committee protocol, in accordance with the Guide for the Care and Use of Laboratory Animals at an AAALAC accredited facility. Rats were acclimated for 48 h prior to any procedures.

Animals within each stage of the study were randomly assigned conditions. Each animal had 4 treatment sites per flank (8 treatment sites per animal). Before procedures, animals were anesthetized with a 3% isoflurane inhalation and shaved along both flanks. After testing for a surgical plane of anesthesia via toe pinch, anesthesia was maintained with 2–3% isoflurane inhalation. A heated surgery table was used to maintain body temperature during the procedure.

2.3. Plasmid DNA

Each treatment site received an intradermal 50 μL injection of 2 mg/mL pDNA. For the GET optimization stage, NTC9385R-Luc-Myc-DDK (Nature Technologies Corporation, Lincoln, NE) was used. This plasmid contained the gene encoding firefly luciferase and was tagged with the myc and DDK tags. For the implant stages of the study animals received NTC9385R-FGF2-Myc-DDK, (Nature Technologies, Lincoln, NE) which encodes for the human FGF2 gene and is and is also tagged with the myc and DDK tags.

2.4. Reporter gene electrotransfer

A platinum tweezer electrode with a 5 mm diameter (BTX, Holliston, MA) and an ELECTROcell B10 pulser (Leroy Biotech, Saint-Orens-de-Gameville, FR) were used to deliver pulses. An intradermal injection of 50 Âμl of 2 mg/ml solution of plasmid DNA was administered to shaved skin on the flank of the animal per treatment site. Skin was then folded between the parallel plated of the tweezer electrode, and pulses were administered. Based on our previous studies [15], monophasic pulses of 60 V applied, 150 ms pulse width, 8 pulses with a 2 mm gap between electrodes was chosen as the starting point for optimization. Using the tweezer electrode with these pulsing conditions resulted in skin damage, therefore, we optimized monophasic conditions in order to reduce either the applied voltage, the applied pulse duration, or the number of pulses to achieve gene delivery and minimize damage. A biphasic condition was also included to minimize twitching, while mimicking the monophasic condition in terms of the time skin is exposed to an electric field (~150 ms × 8 pulses). All electroporation conditions had a 10 s gap between pulses (or in the case of the biphasic pulses, pulse bursts) to avoid potential heating of the electrode. Skin temperature was measured using contactless infrared thermometer. Fig. 2 documents all pulsing conditions used for optimization experiments. Group 1 consisted of a biphasic square wave pulse with a 40 V positive phase for 75 μs, followed by a 150 V negative phase for 20 μs. The gap between the phases was 2 μs long. Eight bursts of 1579 pulses at 5 kHz, with a 10 s gap between bursts to avoid excessive heating of the electrode. Group 2 consisted of a monophasic square wave pulse with a 60 V for 150 ms, with a pulse gap of 10 s for 4 pulses. Group 3 consisted of a monophasic square wave pulse with 60 V for 75 ms, with a pulse gap of 10 s for 8 pulses. Group 4 consisted of a monophasic square wave pulse with 40 V for 150 ms, with a pulse

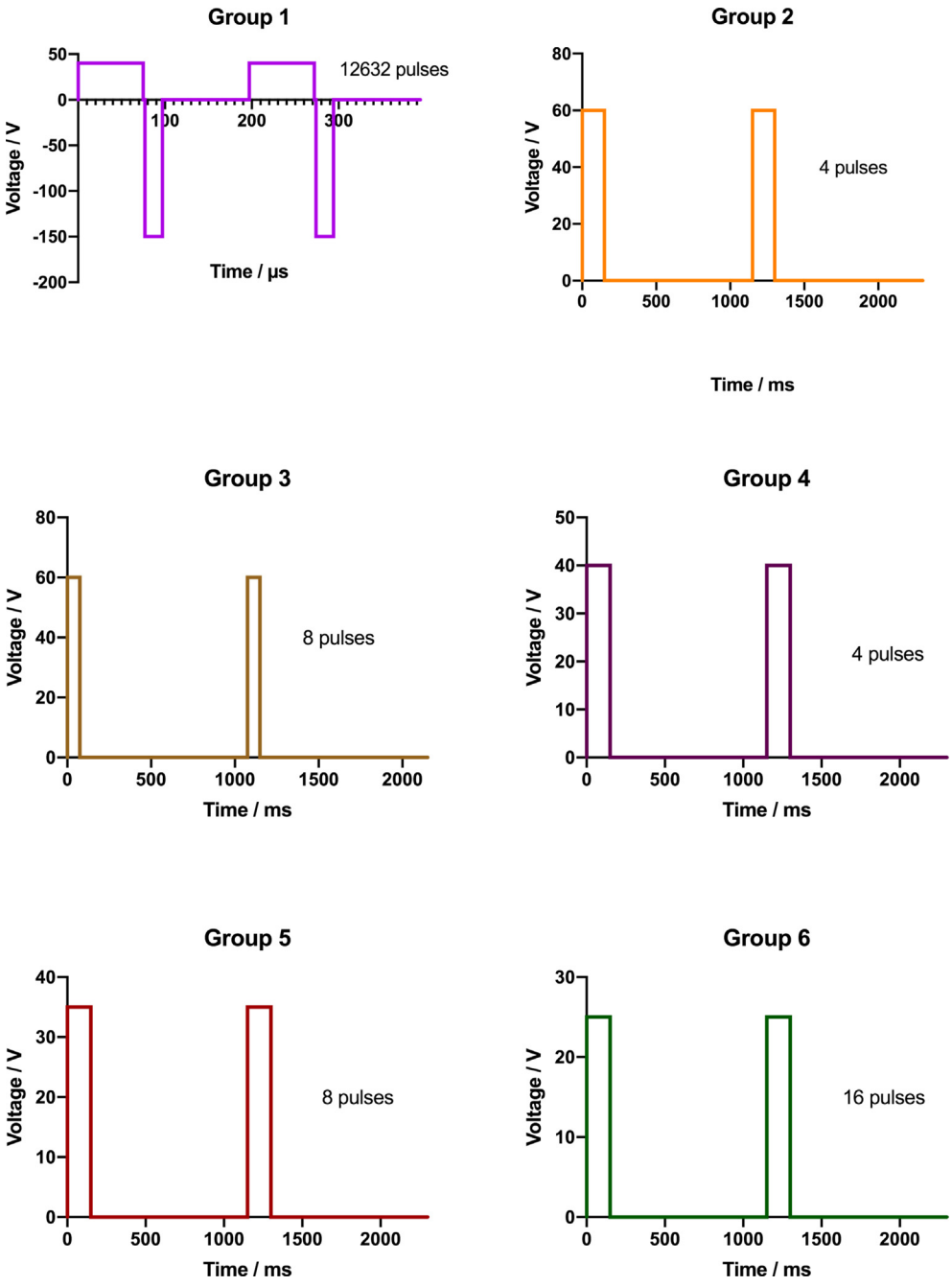

Fig. 2. Pulsing conditions, showing first two pulses. Group 1 consisted of a biphasic square wave pulse with 40 V positive phase for 75 µs, 150 V negative phase for 20 µs, with a 2 µs gap between each phase, and 8 bursts of 1579 pulses, with a 10 s gap between bursts to avoid excessive heating of the electrode (Fig. 2). Group 2 consisted of a monophasic square wave pulse with a 60 V for 150 ms, with a pulse gap of 10 s for 4 pulses. Group 3 consisted of a monophasic square wave pulse with 60 V for 75 ms, with a pulse gap of 10 s for 8 pulses. Group 4 consisted of a monophasic square wave pulse with 40 V for 150 ms, with a pulse gap of 10 s for 4 pulses. Group 5 consisted of a monophasic square wave pulse with 35 V for 150 ms, with a pulse gap of 10 s for 8 pulses. Group 6 consisted of a monophasic square wave pulse with 25 V for 150 ms, with a pulse gap of 10 s for 16 pulses.

gap of 10 s for 4 pulses. Group 5 consisted of a monophasic square wave pulse with 35 V for 150 ms, with a pulse gap of 10 s for 8 pulses. Group 6 consisted of a monophasic square wave pulse with 25 V for 150 ms, with a pulse gap of 10 s for 16 pulses. Groups 1, 4, 5, injection only and negative control (untreated skin) groups have an n = 4 sites and groups 2, 3, and 6 have an n = 8 sites. Based on high levels of expression in epidermis, dermis and underlaying muscle tissue and low levels of damage the Group 1, the biphasic pulsing condition was chosen for the subsequent therapeutic phase of this project.

Animals were monitored after GET for signs of skin damage to the GET sites. Skin damage was assessed at 24 h using a scale 1–5 with 1 being the least severe and 5 being the most severe. Example images of each rating are provided in Fig. 3. The dark, larger circles are drawn with a surgical marker to mark treatment sites. A rating of 1 indicates little to no discoloration of the treatment site, where the skin remains relatively similar to its condition before pulsing. A rating of 2 indicates little discoloration from one area of electrode contact, turning slightly redder than the surrounding skin and no clear circular boundary, leading to a smaller shape

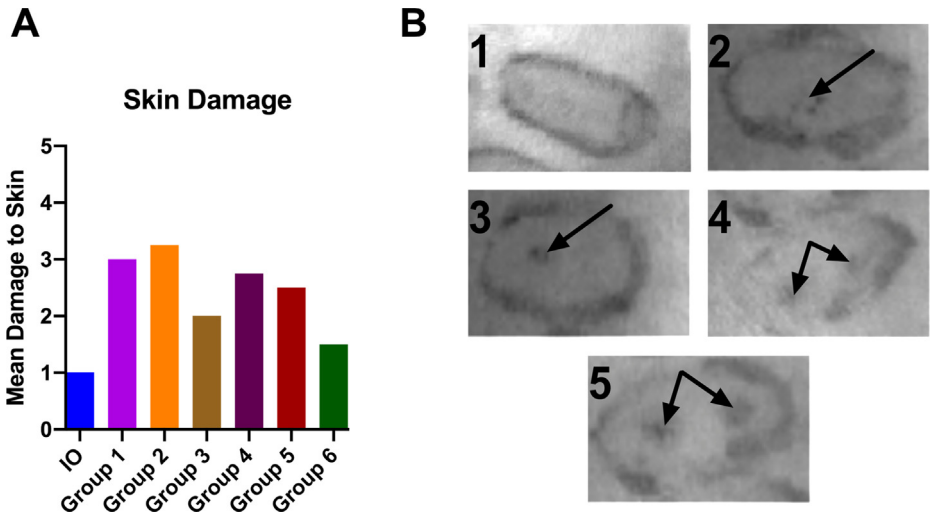

Fig. 3. GET provokes minimal skin damage. (A) Skin damage per group based on semi-quantitative observational data. A score of 1 represents the least damage to skin, with 5 representing most damage. (B) Representative images of the skin damage rating scale used to evaluate GET conditions.

when compared to a "3″ rating. A rating of 3 indicates clear discoloration from one area of electrode contact, with no ambiguity that there is a circular red mark (caused by the circular shape of the electrode) when compared to the surrounding skin. A rating of 4 indicates little discoloration from two areas of electrode contact, allowing similar ambiguity as the "2" rating (no clear circular boundary, smaller size, and not as dark when compared to the next highest rating) and a rating of 5 indicates clear discoloration from two areas of electrode contact (darker and larger than a "4" rating with a clear circular boundary). Skin samples were harvested from the animals at 48 h.

Results from the GET optimization stage were assessed by 3 different factors: damage to tissue, gene expression levels, and distribution of gene expression within different layers of skin tissue. Ultimately, the biphasic condition was used for the subcutaneous implant with FGF2 experiments due to passing threshold for skin damage and gene expression levels, as well as being the only condition where all 3 layers of the skin (epidermis, dermis, and skeletal muscle) had DDK-expressing cells when assessed by immunohistochemistry (IHC).

2.5. Subcutaneous implants and therapeutic gene electrotransfer

For the subcutaneous implant stage, animals were anesthetized with a 3% isoflurane inhalation. After testing for a surgical plane of anesthesia via toe pinch, anesthesia was maintained with 2–3% isoflurane inhalation. A heated surgery table was used to maintain body temperature during the procedure.

Treatment sites were marked using a skin marker and two transverse incisions were made per flank. The skin both posterior and lateral to each incision was separated from the underlying muscle layer via blunt dissection. Acellular scaffolds (Embody, Inc. Norfolk VA) were provided with 6-0 Prolene® sutures secured to each end (Fig. 1A), allowing for the scaffold to be sutured subcutaneously. Then the incision was closed with a 5-0 Monocryl® suture using a subcuticular pattern.

Plasmid DNA was injected into the dermis directly overlaying the scaffold implant, and pulses were administered as follows: a biphasic square wave pulse with 40 V positive phase for 75 μs, 150 V negative phase for 20 μs, with a 2 μs gap between each phase, and 8 bursts of 1579 pulses at 5 kHz, with a 10 s gap between bursts to avoid excessive heating of the electrode (see Fig. 2, group 1). After pulsing animals were allowed to recover from anesthesia and returned to cages. Skin samples were harvested at 48 h. The implant only group had an n = 6 sites and the FGF2 GET group had an n = 6 sites.

2.6. Homogenization and FGF2 ELISA

At 48 h post FGF2 GET animals were humanely euthanized and skin samples of treated and non-treated sites were taken. Samples were homogenized using a Fisherbrand 850 homogenizer. ELISAs for the FGF2 (ab246531, Abcam Cambridge, MA) treatment sites were ran according to manufacturer's (Abcam, Cambridge, MA) instructions. Untreated sites were included in the assay as control for endogenous FGF2 levels.

2.7. Bioluminescence imaging

Animals were imaged to measure bioluminescence levels using the IVIS (Caliper, Perkin-Elmer) at 24 and 48 h after GET. Animals were anesthetized with 3% isoflurane and given subcutaneous injections of D-luciferin at a concentration of 150 mg luciferin/kg of body weight. Each flank was imaged within 5 min after luciferin administration and then returned to their cages and observed until they were fully recovered from anesthesia. Circular ROIs of 1 cm in diameter were used to measure total flux from individual treatment sites.

2.8. Histology evaluation

Sample harvests for histological evaluation were performed on day 2 after GET for reporter gene expression studies. Samples were harvested on day 21 for biocompatibility studies. Skin samples were harvested, fixed in 4% buffered paraformaldehyde and shipped for paraffin-embedding and sectioning by IDEXX BioAnalytics (Westbrook, ME). Hematoxylin and eosin (H&E) staining was also performed by IDEXX BioAnalytics.

Unstained slides were deparaffinized using CitriSolv (Decon Labs, King of Prussia, PA) and an alcohol gradient. Samples were permeabilized using 0.25% Triton X-100 (X100-500ML, Millipore Sigma, St. Louis, MO). Antigen retrieval was performed using citric acid (pH 6). To stain for the DDK protein, a rabbit polyclonal anti-DDK antibody (TA150078, OriGene, Rockville, MD) was used and labeled with an AlexaFluor488 conjugated goat anti-rabbit IgG secondary antibody (A11034, ThermoFisher Scientific, Grand Island,

NY). Negative control samples did not receive a primary antibody. All samples were counterstained with DAPI (5.08741.0001, Millipore Sigma, St. Louis, MO). A Leica (Buffalo Grove, IL) DMi8 microscope was used to perform fluorescent microscopy to take representative images of the epidermis, dermis, and muscle layers.

H&E slides, as stained by IDEXX BioAnalytics (Westbrook, ME), were imaged using a Leica (Buffalo Grove, IL) DMiL microscope. All H&E slides in each group was evaluated for the quantitative aspects of inflammatory response. Plasma cells, lymphocytes, macrophages, foreign body giant cells, and neutrophils were counted using the Image J software. These cells were identified by their characteristic appearance and morphology within the H&E staining by a trained histologist blinded to the experimental groups. Additionally, the number of capillaries between the fibers of the scaffold were also identified morphologically by a trained histologist and counted via Image J (Figure Supplementary figure 1.)

2.9. Statistical analysis

All statistical analysis was completed in GraphPad Prism 9.

Bioluminescent imaging data for the GET optimization were analyzed by using an ordinary two-way ANOVA and Tukey's multiple comparisons test, with $p < 0.05$ considered significant.

H&E staining cell counts were done using Image J. Counts were analyzed by using an ordinary one-way ANOVA and Tukey's multiple comparisons test, with $p < 0.05$ considered significant. These data were also used to calculate inflammation and tissue response per ISO 10993–6:2016(E). Neovascularization was not included in the calculation, as the goal of this study was to enhance early angiogenesis, as hypovascular tissues, such as ligaments and tendons, are known for poor healing.

H&E staining was also used to count the number of blood vessels along the scaffold via Image J. Counts were analyzed by using an unpaired *t* test, with $p < 0.05$ considered significant.

3. Results

3.1. Biofabrication and biocompatibility in vitro

Metabolic activity analysis indicates that fluorescence intensity increased 10-fold from day 1 to day 7, indicating an increase in cellular metabolism and proliferation (Fig. 1B). Additionally, fluorescent imaging (Fig. 1C, D) shows bright autofluorescence of the collagen fiber at 405 nm (blue) and allows for clear visualization of DiD-labeled tenocytes attachment throughout the scaffold (magenta).

3.2. Gene electrotransfer optimization

The mean damage rating between all GET groups is 2.5 (Fig. 3 A). Example images of the scale for skin damage are shown, with 5 being the most severe damage observed (Fig. 3B). A more descriptive definition of each of the ratings is provided in Section 3.2. The mean damage rating for group 1, which was used in the therapeutic portion of the study, was 3. The maximum accepted damage to the skin for the therapeutic stage of the study was 3. Additionally, there is no damage to the skin in GET treatment sites that were also analyzed for gene expression via IHC (Fig. 4B).

Group 1 had significantly higher levels of expression over plasmid DNA injection only ($p < 0.0273$, Fig. 4A) and was the only group that had expression in the epidermis, dermis, and skeletal muscle layers (Fig. 4C–E). While group 3 also exhibited significantly higher levels of expression, (Fig. 4A) the expression was largely confined to the skeletal muscle. For other conditions, DDK-expressing cells were only present in either the epidermis, dermis, hypodermis or muscle. The IO group largely did not have detectable DDK-expressing cells, with none to minimal expression observed in the epidermis (Fig. 4F), while no expression was observed in the dermis or the muscle layers of the skin (Fig. 4G and H). Other groups had differing distributions, which are briefly described in the following: Groups 2, 3, and 6 only had notable expression in the muscle layer, Group 4 only had notable expression in the dermis, and Group 5 only had notable expression in the epidermis.

3.3. FGFs GET improved in vivo biocompatibility

FGF2 GET groups had protein concentration significantly higher than the IO group when measured via ELISA. Samples were also taken from sites that were not injected with the FGF2 pDNA, and had significantly lower FGF2 protein concentration when compared to the IO group and FGF2 GET groups (Fig. 5A). Additionally, DDK-expressing cells were found in the epidermis, dermis, and muscle layers of the skin for the GET group (Fig. 5B–D). The IO group largely did not have detectable DDK-expressing cells, with few detected in the dermis on day 21 (Fig. 5E–G).

The scaffold was also able to be visualized in H&E staining for both the GET group (Figs. 6A, 7 B, Supplemental Fig. 1A) and the implant only group (Figs. 6B, 7C, Supplemental Fig. 1B).

Skin damage was evaluated semi quantitatively on day 1 post GET, with the most severe damage (full thickness, involvement of the entire treatment zone) assigned 5, and no damage assigned a score of 1 (Fig. 3B). A score of 2 and 3 indicated some discoloration, while a 4 indicated the presence of a scab. We did not observe much notable damage, and skin discoloration was often the most severe outcome. Therefore, we conclude that the GET conditions selected are safe for therapeutic gene delivery to the skin.

In the FGF2 GET treatment sites there were significantly fewer foreign body giant cells, plasma cells, and lymphocytes when compared to the implant only animals at day 21 (Fig. 6), showing that GET of FGF2 attenuates chronic inflammation and foreign body responses. However, there was no significant difference between the two groups when counting neutrophils or macrophages indicating no acute inflammation, as these are the cell types that arrive first. Inflammation was assessed per ISO 10993–6:2016(E), excluding neovascularization from the calculation. The ISO inflammation rating for the FGF2 GET group was 0, and the rating for the implant only group was 1.334. Both are in the "minimal or no reaction" category.

Blood vessel counts also revealed that there was a significant increase in the amount of blood vessels when comparing the GET group to the implant only group (Fig. 7), suggesting that GET of FGF2 can significantly enhance angiogenesis within a biomanufacturing tissue analog designed for tendon repair.

4. Discussion

The DiD-labeled tenocytes were largely evenly distributed along the scaffold due to the bioprinting process used. The alamarBlue assay also revealed that the tenocytes were viable and proliferated on the scaffolds after the bioprinting process. This is significant as the scaffold provides a favorable environment for tenocyte proliferation and is not cytotoxic either during bioprinting or subsequent cell culture. These results lead us to test the scaffold *in vivo*.

It has been previously shown that high frequency biphasic pulses reduce muscle twitching during irreversible electroporation of tumor tissue [18,19]. This is beneficial for applications to the

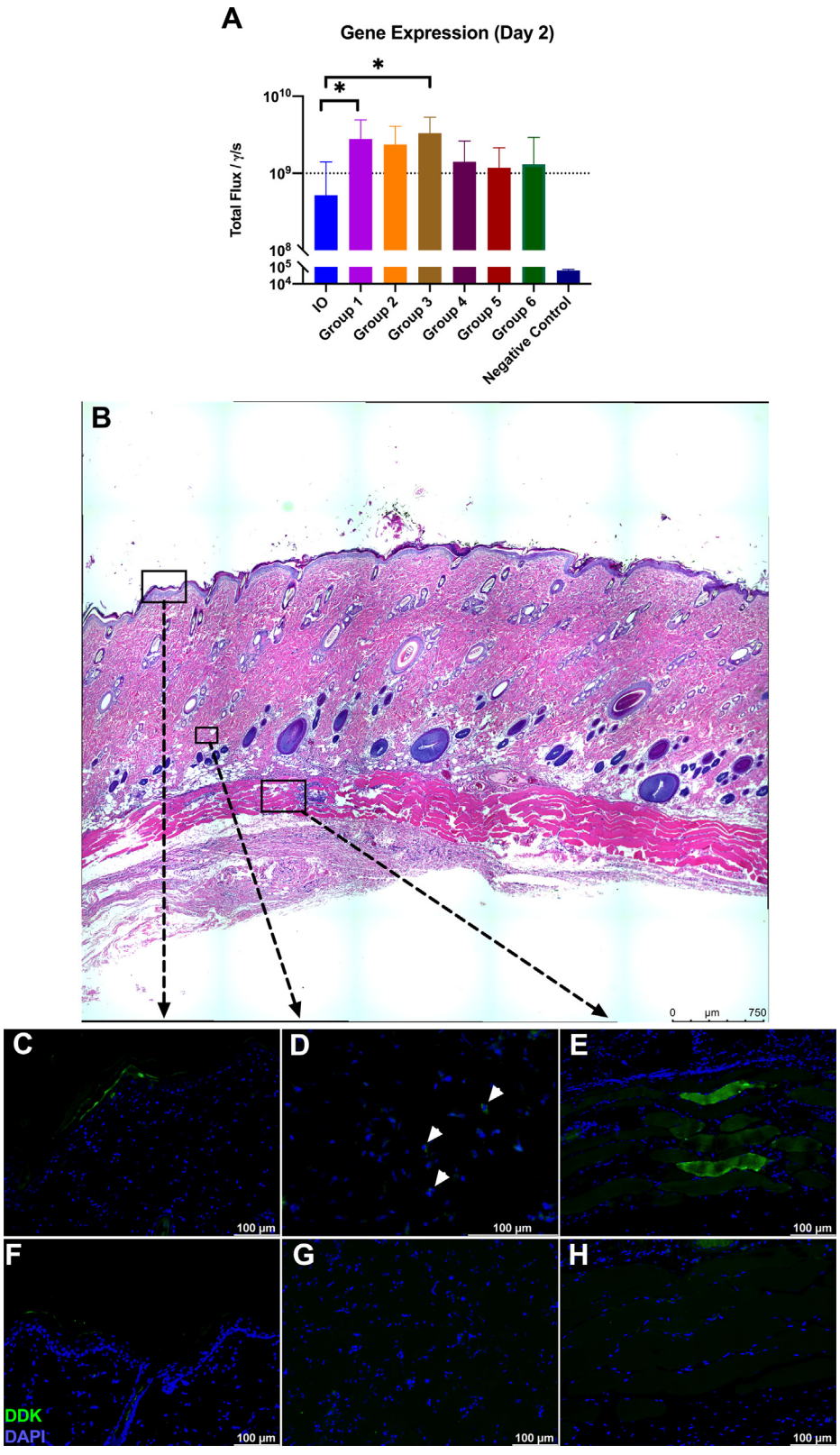

Fig. 4. Biphasic GET enhances gene expression in the epidermis, dermis and the underlaying muscle. Biphasic GET (group 1) compared to IO had significantly higher expression levels, $p < 0.0273$ (A). H&E of the GET group (group 1) showing no damage to the skin (B). Group 1 IF of epidermis layer (C). Group 1 IF of dermis layer with arrows pointing to DDK-expressing cells (D). Group 1 IF of skeletal muscle layer (E). IO IF of the epidermis layer (F). IO IF of the dermal layer (G). IO IF of the skeletal muscle layer (H).

skin, and other tissues, to maintain contact of the electrode with the tissue. However, this is particularly important in excitable cells, such as the cardiomyocytes, to avoid potential issues with fibrillation during gene delivery. Although we have previously established monophasic conditions that successfully delivered transgenes to the skin, we aimed to explore biphasic conditions

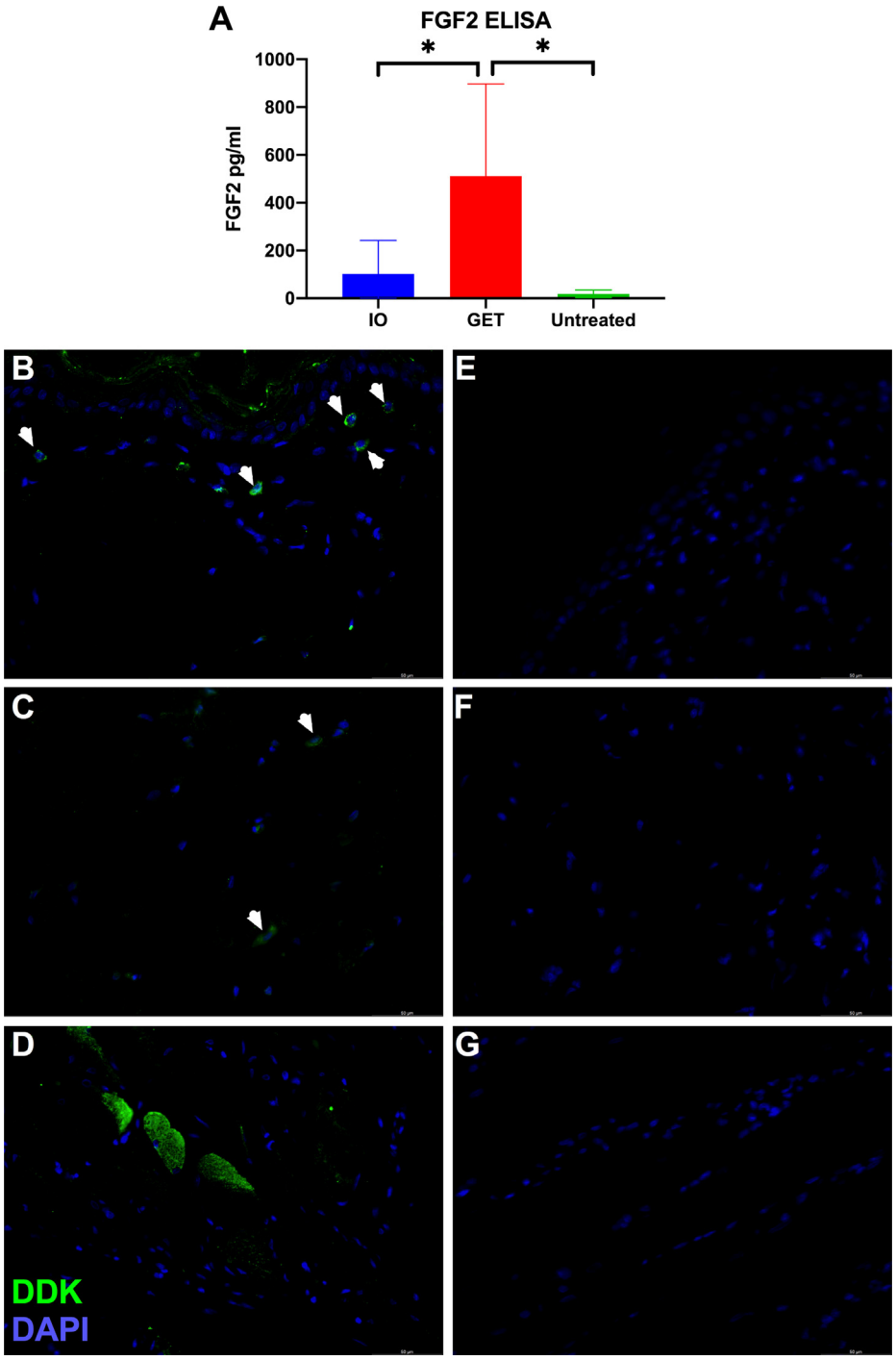

Fig. 5. FGF2 protein expression is significantly higher using GET, and observed in all layers of the skin. (A) FGF2 ELISA reveals that the protein concentration of FGF2 is significantly higher in the GET group when compared to both the untreated and IO groups. * $p < 0.001$. IF for the FGF2 GET animals. DDK staining (green) and DAPI (blue) showing DDK expressing cells in the FGF2 GET group (B) epidermis, (C) dermis, and (D) muscle layers. IF of the implant only group (E) epidermis, (F) dermis, and (G) muscle layers. (For interpretation of the references to colour in this figure legend, the reader is referred to the web version of this article.)

as well [15]. This, combined with the discovery of a biphasic condition that caused expression in all layers of the skin, lead us to choose a biphasic condition for our therapeutic gene delivery.

The biphasic GET condition provided high levels of gene expression and could be used for other applications in which gene delivery to the skin is necessary. In comparison, another study using GET for gene delivery to the skin required heating of the area to get similar expression levels [15]. While reporter gene expression was favorable, we confirmed these results by measuring FGF2 protein levels at 2 days post GET, with ELISA, indicating significantly higher protein levels than endogenous FGF or IO groups (Fig. 5). Additionally, the biphasic FGF2 gene delivery resulted in DDK-expressing cells in epidermis, dermis, and muscle (Fig. 5).

Surprisingly, we also found that different pulsing conditions resulted in transgene expression in different layers of the skin. While gene delivery to all three layers of the skin was considered optimal in this study, delivering gene therapy to only a subset of cells has clinical significance and could be applied to diseases such

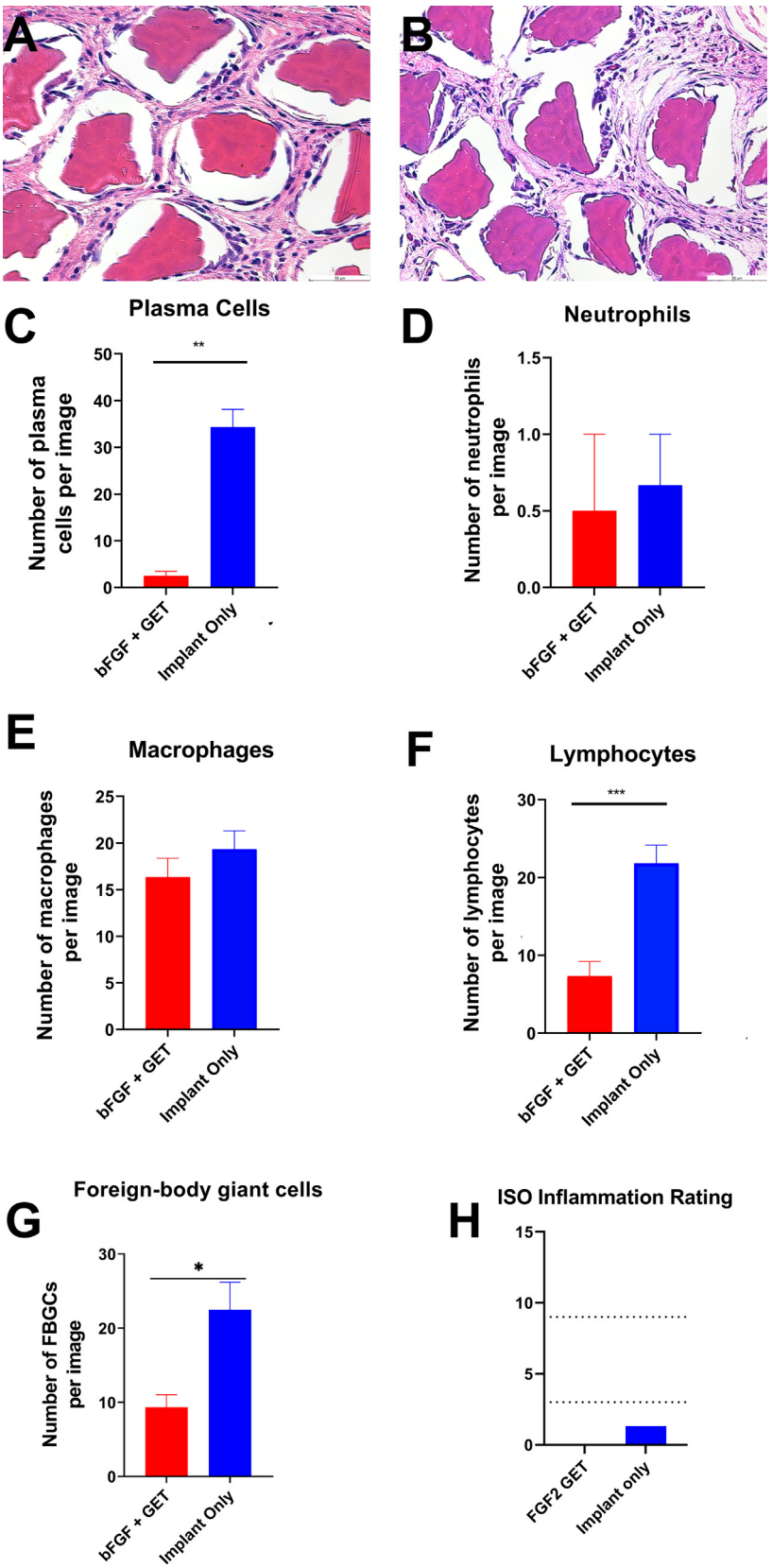

Fig. 6. FGF2 GET increases biocompatibility of the scaffold. H&E of the (A) FGF2 GET group and (B) implant only group, harvest at day 21. Cell counts for the FGF2 and implant only groups per image of 0.55 mm^2 (C) plasma cells, (D) neutrophils, (E) macrophages, (F) lymphocytes, and (G) foreign body giant cells. (H) ISO standardized inflammation rating. The dotted lines represent the thresholds between minimal and slight reaction (bottom) and slight reaction and moderate reaction. The scale cut-off is the threshold for severe reaction. $^{*}p < 0.05$, $^{**}p < 0.01$, $^{***}p < 0.001$.

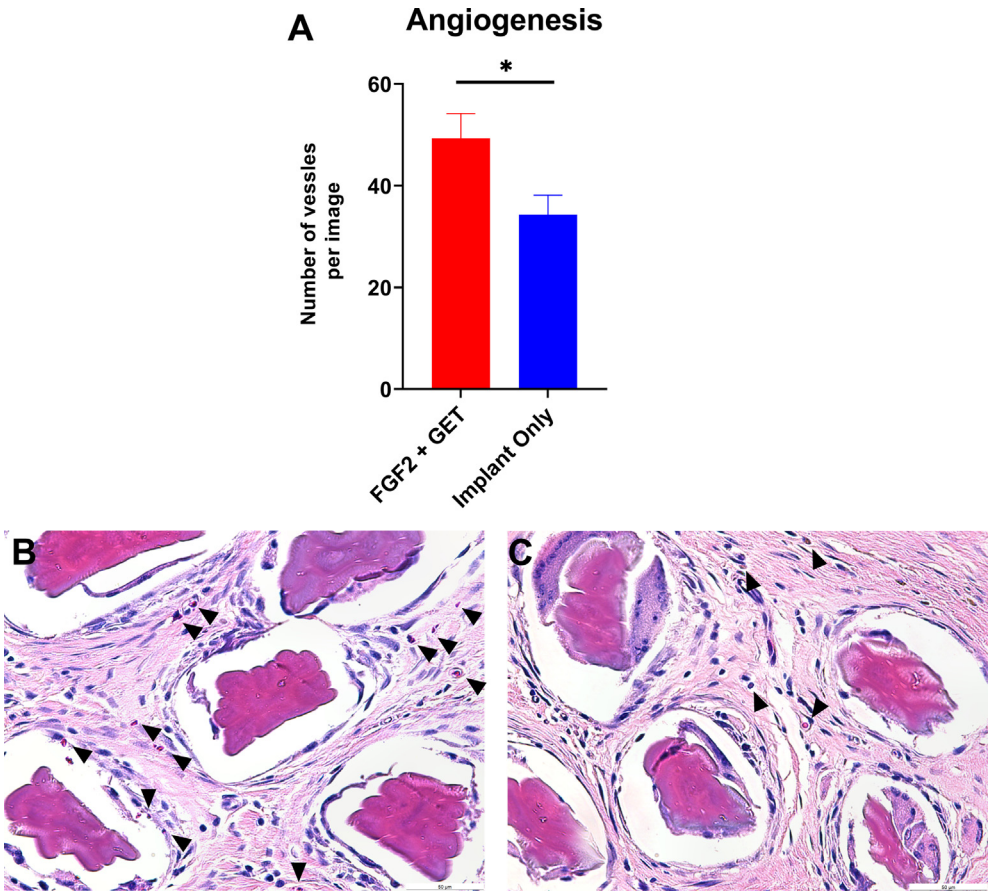

Fig. 7. GET of FGF2 significantly increased angiogenesis. (A) Counts of the blood vessels per group per image of 0.55 mm^2. *$p < 0.05$. H&E staining of the (B) FGF2 GET and (C) implant only groups. Vessels are indicated by black arrows.

as cancer. One example of this is a monophasic condition that consists of 40 V, a 150 ms pulse width, a 10 s pulse gap, and 8 pulses, which only achieved gene delivery to the epidermis. Gene delivery specific to the epidermis using GET, however, has been previously reported in other studies [15]. Unique to our study, we discovered conditions in which gene delivery was limited to the dermis (group 4) or the muscle (group 6) layer of the skin. Further research could potentially apply this concept to different tissue types to target specific cells during gene therapy.

The form of hyaluronic acid used as a fiber binder or glue is known to illicit a mild inflammatory response, common to most all foreign materials implanted into the body. We also found that there were immunological benefits to combining FGF2 GET with the scaffold. Namely, delivering FGF2 via GET enhanced biocompatibility in terms of reduced foreign body response at 3 weeks. Plasma cells, lymphocytes, and foreign body giant cells, which were significantly reduced in the FGF2 GET groups, are all associated with inducing inflammation [31–33]. Plasma cells in particular are known for inducing inflammation and producing antibodies as part of the immune response [33]. Lymphocytes are an important determiner of biocompatibility, as they contribute to inflammation, immune response, and the foreign body response [32], all of which are significant in assessing biocompatibility. Foreign body giant cells are cells that are associated with inflammation and foreign body response and are formed via macrophage fusion [31]. Reducing the number of foreign body giant cells may also be beneficial in preventing premature degradation of the scaffold, as the recruitment of foreign body giant cells caused some biomaterials such as polylactides [34] and polycarbonates [35] to degrade. During harvest of skin samples, we were still able to identify the scaffold, which was intact at 21 days. We did not observe degradation of the scaffold. The significant reduction of plasma cells, lymphocytes, and foreign body giant cells in the FGF2 GET group suggests that FGF2 GET enhances biocompatibility by reducing the number of cell involved in inflammation [31–33], immune response [32], foreign body response[31,32]. Additionally, no acute inflammation was observed at the 3-week time point, as no significant presence of neutrophils or macrophages was detected.

We were able to observe that the significant differences in the cell types discussed above did not result in a difference of inflammation when measure by ISO 10993–6:2016(E). This suggests that although our cell counts were significantly different for some cell types associated with inflammation, both groups did not see a chronic inflammatory response as characterized by the ISO. This lack of chronic inflammatory response, with both groups falling into the "minimal or no reaction" category, suggests that the collagen scaffold is highly biocompatible, particularly when combined with FGF2 GET, which had an ISO rating of 0.

Delivery of FGF2 significantly increased angiogenesis when compared to the implant-only animals. Since angiogenesis is a critical part of tissue remodeling and repair [11], gene therapy of angiogenesis-linked genes, such as FGF2, could potentially reduce recovery time with accelerated tendon healing when delivered in a defect model. This is particularly important in tendinopathy, as recovery typically takes up to 3–12 month, and during this time patients cannot bear weight on the tendon [8].

5. Conclusion

The microfluidically wet-extruded collagen grafts provide a favorable microenvironment for cell attachment, cell proliferation and elicit minimal inflamatory response. By optimizing GET conditions, we were able to minimize skin damage and deliver a therapeutic gene resulting in significantly higher protein concentration and cells expressing the protein in three different layers of the skin. Additionally, intradermal FGF2 gene delivery was able to reduce localized foreign body responses to subcutaneously implanted collagen scaffolds. FGF2 GET enhanced angiogenesis, which may play a role in reduction of chronic inflammation and foreign body response. Due to these factors, the combination of the collagen scaffold and GET could potentially aid in the treatment of tendon injury.

Declaration of Competing Interest

The authors declare the following financial interests/personal relationships which may be considered as potential competing interests: Dr. Michael Francis is the CSO of Embody Inc. where the collagen scaffold used in this study was developed.

Acknowledgments

This work was in part supported by a research grant from the Virginia Biosciences Health Research Corporation Catalyst. The authors would like to thank Richard Heller for use of his laboratory space and equipment and the SoBran vivarium staff.

Appendix A. Supplementary material

Supplementary data to this article can be found online at https://doi.org/10.1016/j.bioelechem.2021.107980.

References

[1] S. Houshian, T. Tscherning, P. Riegels-Nielsen, The epidemiology of achilles tendon rupture in a danish county, Injury 29 (1998) 651–654.
[2] J. Leppilahti, J. Puranen, S. Orava, Incidence of achilles tendon rupture, Acta Orthop. Scand. 67 (1996) 277–279.
[3] T.T. Huttunen, P. Kannus, C. Rolf, L. Fellander-Tsai, V.M. Mattila, Acute achilles tendon ruptures: Incidence of injury and surgery in sweden between 2001 and 2012, Am. J. Sports Med. 42 (2014) 2419–2423.
[4] I. Lantto, J. Heikkinen, T. Flinkkila, P. Ohtonen, J. Leppilahti, Epidemiology of achilles tendon ruptures: Increasing incidence over a 33-year period, Scand. J. Med. Sci. Sports 25 (2015) e133–e138.
[5] A. Ganestam, T. Kallemose, A. Troelsen, K.W. Barfod, Increasing incidence of acute achilles tendon rupture and a noticeable decline in surgical treatment from 1994 to 2013. A nationwide registry study of 33,160 patients, Knee Surg. Sports Traumatol. Arthrosc. 24 (2016) 3730–3737.
[6] Y. Yasui, I. Tonogai, A.J. Rosenbaum, Y. Shimozono, H. Kawano, J.G. Kennedy, The risk of achilles tendon rupture in the patients with achilles tendinopathy: Healthcare database analysis in the united states, Biomed. Res. Int. 2017 (2017), 7021862-7021862.
[7] A.C. Egger, M.J. Berkowitz, Achilles tendon injuries, Curr. Rev. Musculoskeletal Med. 10 (2017) 72–80.
[8] X. Yang, H. Meng, Q. Quan, J. Peng, S. Lu, A. Wang, Management of acute achilles tendon ruptures: a review, Bone Joint Res. 7 (2018) 561–569.
[9] T. Waitayawinyu, P.A. Martineau, S. Luria, D.P. Hanel, T.E. Trumble, Comparative biomechanic study of flexor tendon repair using fiberwire, J. Hand Surg. Am. 33 (2008) 701–708.
[10] N. Maffulli, F. Spiezia, E. Pintore, U.G. Longo, V. Testa, G. Capasso, V. Denaro, Peroneus brevis tendon transfer for reconstruction of chronic tears of the achilles tendon: a long-term follow-up study, J. Bone Joint Surg. Am. 94 (2012) 901–905.
[11] K. Lipman, C. Wang, K. Ting, C. Soo, Z. Zheng, Tendinopathy: Injury, repair, and current exploration, Drug Des., Develop. Therapy 12 (2018) 591–603.
[12] C. Gabler, J.-O. Saß, S. Gierschner, T. Lindner, R. Bader, T. Tischer, In vivo evaluation of different collagen scaffolds in an achilles tendon defect model, Biomed Res. Int. 2018 (2018), 6432742-6432742.
[13] A.D. Nocera, R. Comín, N.A. Salvatierra, M.P. Cid, Development of 3d printed fibrillar collagen scaffold for tissue engineering, Biomed. Microdevices 20 (2018) 26.
[14] T. Wirth, N. Parker, S. Yla-Herttuala, History of gene therapy, Gene 525 (2013) 162–169.
[15] A. Bulysheva, J. Hornef, C. Edelblute, C. Jiang, K. Schoenbach, C. Lundberg, M.A. Malik, R. Heller, Coalesced thermal and electrotransfer mediated delivery of plasmid DNA to the skin, Bioelectrochemistry 125 (2019) 127–133.
[16] R. Heller, Y. Cruz, L.C. Heller, R.A. Gilbert, M.J. Jaroszeski, Electrically mediated delivery of plasmid DNA to the skin, using a multielectrode array, Hum. Gene Ther. 21 (2010) 357–362.
[17] A. Donate, A. Bulysheva, C. Edelblute, D. Jung, M.A. Malik, S. Guo, N. Burcus, K. Schoenbach, R. Heller, Thermal assisted in vivo gene electrotransfer, Curr. Gene Ther. 16 (2016) 83–89.
[18] B. Mercadal, C.B. Arena, R.V. Davalos, A. Ivorra, Avoiding nerve stimulation in irreversible electroporation: a numerical modeling study, Phys. Med. Biol. 62 (2017) 8060–8079.
[19] C.B. Arena, M.B. Sano, J.H. Rossmeisl, J.L. Caldwell, P.A. Garcia, M.N. Rylander, R. V. Davalos, High-frequency irreversible electroporation (h-fire) for non-thermal ablation without muscle contraction, Biomed. Eng. Online 10 (2011) 102.
[20] A.A. Bulysheva, R. Heller, 3d culture models to assess tissue responses to electroporation, in: D. Miklavčič (Ed.), Handbook of electroporation, Springer International Publishing, Cham, 2017, pp. 437–450.
[21] L. Wasungu, J.M. Escoffre, A. Valette, J. Teissie, M.P. Rols, A 3d in vitro spheroid model as a way to study the mechanisms of electroporation, Int. J. Pharm. 379 (2009) 278–284.
[22] E. Sieni, M. Dettin, M. De Robertis, B. Bazzolo, M.T. Conconi, A. Zamuner, R. Marino, F. Keller, L.G. Campana, E. Signori, The efficiency of gene electrotransfer in breast-cancer cell lines cultured on a novel collagen-free 3d scaffold, Cancers (Basel) 12 (2020).
[23] P. Brun, M. Dettin, L.G. Campana, F. Dughiero, P. Sgarbossa, C. Bernardello, A.L. Tosi, A. Zamuner, E. Sieni, Cell-seeded 3d scaffolds as in vitro models for electroporation, Bioelectrochemistry 125 (2019) 15–24.
[24] K. Znidar, M. Bosnjak, M. Cemazar, L.C. Heller, Cytosolic DNA sensor upregulation accompanies DNA electrotransfer in b16.F10 melanoma cells, Mol Ther Nucleic Acids 5 (2016) e322.
[25] T. Rodrigues, B. Kundu, J. Silva-Correia, S.C. Kundu, J.M. Oliveira, R.L. Reis, V.M. Correlo, Emerging tumor spheroids technologies for 3d in vitro cancer modeling, Pharmacol. Ther. 184 (2018) 201–211.
[26] E. Imai, Y. Isaka, Gene electrotransfer: Potential for gene therapy of renal diseases, Kidney Int. 61 (2002) S37–S41.
[27] M.P. Ho, Tissue engineering with electroporation, in: D. Miklavcic (Ed.), Handbook of electroporation, Springer International Publishing, Cham, 2016, pp. 1–21.
[28] Y.R. Yun, J.E. Won, E. Jeon, S. Lee, W. Kang, H. Jo, J.H. Jang, U.S. Shin, H.W. Kim, Fibroblast growth factors: Biology, function, and application for tissue regeneration, J. Tissue Eng. 2010 (2010) 218142.
[29] B. Ferraro, Y.L. Cruz, M. Baldwin, D. Coppola, R. Heller, Increased perfusion and angiogenesis in a hindlimb ischemia model with plasmid fgf-2 delivered by noninvasive electroporation, Gene Ther. 17 (2010) 763–769.
[30] S. Nishikage, H. Koyama, T. Miyata, S. Ishii, H. Hamada, H. Shigematsu, In vivo electroporation enhances plasmid-based gene transfer of basic fibroblast growth factor for the treatment of ischemic limb, J. Surg. Res. 120 (2004) 37–46.
[31] J.M. Anderson, A. Rodriguez, D.T. Chang, Foreign body reaction to biomaterials, Semin. Immunol. 20 (2008) 86–100.
[32] J.M. Anderson, A.K. Mcnally, Biocompatibility of implants: Lymphocyte/macrophage interactions, Semin. Immunopathol. 33 (2011) 221–233.
[33] P.D. Pioli, Plasma cells, the next generation: beyond antibody secretion, Front. Immunol. 10 (2019).
[34] Y. Tokiwa, B.P. Calabia, Biodegradability and biodegradation of poly(lactide), Appl. Microbiol. Biotechnol. 72 (2006) 244–251.
[35] R.S. Labow, E. Meek, J.P. Santerre, Hydrolytic degradation of poly(carbonate)-urethanes by monocyte-derived macrophages, Biomaterials 22 (2001) 3025–3033.
[36] A. Dasgupta, N. Sori, S. Petrova, Y. Maghdouri-White, N. Thayer, N. Kemper, D. Leathers, K. Coughenour, J. Dascoli, R. Palikonda, C. Donahue, A.A. Bulysheva, M.P. Francis, Comprehensive collagen crosslinking comparison of microfluidic wet-extruded microfibers for bioactive surgical suture development, Acta Biomater. 128 (2021) 186–200, https://doi.org/10.1016/j.actbio.2021.04.028.